JCI The Journal of Clinical Investigation

CLIC1 recruits PIP5K1A/C to induce cell-matrix adhesions for tumor metastasis

Jei-Ming Peng, … , Ming-Chin Yu, Sen-Yung Hsieh

J Clin Invest. 2020. https://doi.org/10.1172/JCI133525.

Research In-Press Preview **Cell biology** **Hepatology**

Graphical abstract

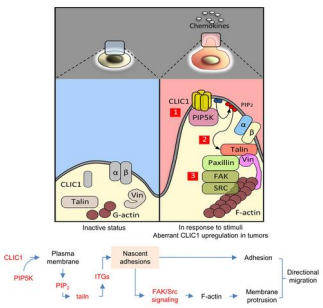

CLIC1 recruits PIP5K1A/C to induce cell-matrix adhesions for tumor metastasis

Jei-Ming Peng[1,2†], Sheng-Hsuan Lin[1†], Ming-Chin Yu[3], and Sen-Yung Hsieh[1,4]*

[1]Department of Gastroenterology and Hepatology, Chang Gung Memorial Hospital, Linkou, Taoyuan 333, Taiwan

[2]Institute for Translational Research in Biomedicine, Kaohsiung Chang Gung Memorial Hospital, Kaohsiung 833, Taiwan

[3]Department of General Surgery, Chang Gung Memorial Hospital, Linkou, Taoyuan 333, Taiwan

[4]Chang Gung University College of Medicine, Taoyuan 333, Taiwan

[†]JMP and SHL: contributing equally to this study

Running title: CLIC1 directs membrane protrusion and cell-matrix adhesion

Conflict of interest: The authors have declared that no conflict of interest exists.

***Correspondence:** Dr. Sen-Yung Hsieh, Department of Gastroenterology and Hepatology, Chang Gung Memorial Hospital, Taoyuan 333, Taiwan; Cell-phone: 886-975368031; Fax: 886-3-3272236; E-mail: siming@cgmh.org.tw; siming.shia@msa.hinet.net

Abstract

Membrane protrusion and adhesion to the extracellular matrix, which involves the extension of actin filaments and formation of adhesion complexes, are the fundamental processes for cell migration, tumor invasion, and metastasis. How cancer cells efficiently coordinate these processes remains unclear. Here, we showed that membrane-targeted CLIC1 spatiotemporally regulates the formation of cell-matrix adhesions and membrane protrusions through the recruitment of PIP5Ks to the plasma membrane. Comparative proteomics identified CLIC1 upregulated in human hepatocellular carcinoma (HCC) and associated with tumor invasiveness, metastasis, and poor prognosis. In response to migration-related stimuli, CLIC1 recruited PIP5K1A and PIP5K1C from the cytoplasm to the leading edge of the plasma membrane, where PIP5Ks generate a PIP_2-rich microdomain to induce the formation of integrin-mediated cell-matrix adhesions and the signaling for cytoskeleon extension. CLIC1 silencing inhibited the attachment of tumor cells to culture plates and the adherence and extravasation in the lung alveoli resulting in suppressed lung metastasis in mice. This study reveals an unrecognized mechanism that spatiotemporally coordinates the formation of both lamellipodium/invadopodia and nascent cell-matrix adhesions for directional migration and tumor invasion/metastasis. The unique traits of upregulation and membrane targeting of CLIC1 in cancer cells make it an excellent therapeutic target for tumor metastasis.

Keywords

chloride intracellular channel 1, cell-matrix adhesion, directional migration, invadopodia, invasion, lamellipodia, metastasis, nascent adhesions, PIP5K, spatiotemporal regulation of lamellipodia

Brief summary:

CLIC1 recruits PIP5Ks to the plasma membrane to initiate "PIP_2-talin-integrin" signaling for cell-matrix adhesion formation and signaling, spatiotemporally regulating lamellipodia and invadopodia for tumor metastasis.

Introduction

Membrane protrusion and adhesion to the extracellular matrix are the two fundamental processes of different modes of cell migration, which are crucial for embryonic development, wound healing, immune responses, and tumor invasion and metastasis (1, 2). Membrane protrusion, a *de novo* membrane extension in the direction of movement forming the leading edge as filopodia, lamellipodia, or invadopodia, results from the expansion of the cytoskeleton (actin filaments or F-actin, which serves as a scaffold for myosin II motors and other effectors). Adhesion to the extracellular matrix occurs through the formation of adhesion complexes, namely cell-matrix adhesions. Cell-matrix adhesions are membranous hubs that mediate the interaction between the extracellular matrix and the cellular scaffolding and signaling machinery via membranous receptors, mainly integrins, for extracellular ligands. Integrins, a large superfamily of heterodimeric receptors, bind to diverse extracellular matrix molecules to trigger intracellular signals (3, 4). Talin is required for most integrin-mediated adhesive functions (5, 6) and is thus viewed as a central player in integrin functions, such as adhesion for migration (7, 8). Binding of talin to the cytoplasmic domain of integrin β leads to the formation of integrin $\alpha\beta$ heterodimers, resulting in the assembly of nascent cell-matrix adhesions, which then elicit adhesion-mediated signals regulating actin cytoskeleton polymerization and cell motility (9). Therefore, the formation of nascent cell-matrix adhesions plays a pivotal role in cell adherence to the matrix and signaling for extension of the actin cytoskeleton during cell migration (10). Interestingly, accumulating evidence suggests the

involvement of deregulated cell-matrix adhesions in cancer development and tumor metastasis (11, 12). However, how cells, particularly tumor cells with high invasiveness, spatiotemporally regulate cell-matrix adhesion and the formation of filopodia, lamellipodia, and invadopodia for directional migration remains unclear.

The chloride intracellular channel (CLIC) family consists of six highly conserved members (CLIC1-6). All CLICs consist of an N-terminal thioredoxin-like domain followed by an α-helix C-terminal domain (13). The CLICs are unique among eukaryotic ion channels in that they can exist as either a soluble monomer or an integral membrane channel upon undergoing structural rearrangement (14). These proteins play diverse physiological roles in health and diseases, including inflammatory responses to tissue injury and tumor progression (15). CLIC1 is the most studied because of its broad expression in different mammalian tissues and cells (16). In response to stimuli, such as oxidative stress, CLIC1 changes its structure and is inserted into lipid membranes to form an ion channel in vitro (14, 17, 18). In macrophages, CLIC1 inserts into the phagosomal membrane upon phagocytosis. Increasing evidence has shown that CLIC1 can insert into the plasma membrane (19) and function as a chloride ion channel (20), although these findings are still in debation. CLIC1 is widely upregulated in many types of human cancers (21-26) and is associated with tumor progression and metastasis (22, 27, 28). However, the involvement of CLIC1 in tumor progress and metastasis has not been fully elucidated.

Here, we demonstrate that CLIC1 is progressively upregulated along with the progression of

human hepatocellular carcinoma (HCC) and associated with tumor metastasis. In response to chemotaxic or mechanotaxic stimuli, CLIC1 recruited PIP5Ks to the leading edge of the plasma membrane, where it generates phosphatidylinositol 4,5-bisphosphate (PIP_2) and subsequently activation of talin and integrin $\alpha4\beta1$ and $\alpha6\beta4$ to initiate the assembly of nascent cell-matrix adhesions and adhesion-mediated signaling for actin cytoskeleton remodeling to form lamellipodia and invadopodia. CLIC1 deletion suppressed the formation of nascent adhesions and signaling of tumor cells in vitro and tumor metastasis in vivo. Our findings suggest CLIC1 as a potential therapeutic target for cancer invasion and metastasis.

Results

Comparative proteomics identified CLIC1 progressive upregulated along with HCC progress. Hepatocellular carcinoma (HCC) is highly invasive (29). To identify proteins contributing to the high invasiveness of HCC, we compared the protein profiles in seven normal liver, 12 early HCC (solitary tumor < 3 cm without invasion), and 13 invasive HCC samples (invading into major branches of the portal or hepatic veins; Supplemental Table 1) by using two-dimensional gel electrophoresis (2-DE; Figure 1A). A total of 1238 spots matched across gels and 104 proteins were identified (Supplemental Table 2). Of them, CLIC1 was the only one that was progressively upregulated along with tumor progression (relative level: normal liver/early HCC/invasive HCC = 1/4.65/10.09, P< 0.001; Figure 1B-C; Supplemental Table 2). We thus selected CLIC1 for further investigation.

CLIC1 upregulation in HCC is associated with vascular invasion, metastasis, and lower survival

To validate the correlation between CLIC1 upregulation and HCC progression, we used immunohistochemistry (IHC) to compare the CLIC1 levels between the HCC tissues (T) and the para-tumor liver tissues (N) on tissue microarrays (TMA) from 89 patients of HCC (Supplemental Figure 1A and Supplemental Table 3). The CLIC1 level was significantly increased in the HCC tissues ($P <$ 0.001 by Student's t and paired t-tests; Figure 2A). Moreover, high CLIC1 levels were significantly associated with advanced tumor stages (P = 0.006, Kruskal-Wallis test), higher vascular invasion status (P = 0.018, Kruskal-Wallis test; Table1), and a lower survival rate (P = 0.008, log-rank test; Figure 2B). We further compared the CLIC1 levels between the paired primary and metastatic HCC samples from 12 patients (Supplemental Figure 1B). We found significantly higher CLIC1 levels in the metastatic HCC samples than the primary HCC samples (P = 0.019, t-test and <0.001, paired t-test; Figure 2C).

To consolidate the above findings, we retrieved an HCC cohort from The Cancer Genome Atlas (TCGA, https://cancergenome.nih.gov/) database. We found that progressive CLIC1 upregulation was along with higher tumor stages (P = 0.0014; Figure 2D). Moreover, high CLIC1 expression was associated with lower survival (P < 0.001; Figure 2E).

Considering that pancreas and lung cancers are highly invasive, we retrieved a cohort of pancreatic ductal adenocarcinoma (PDAC, n = 177) and a cohort of nonsmall-cell lung cancer

(NSCLC, n = 513) from TCGA datasets. We found that high CLIC1 expression was significantly associated with lower survival in both cohorts ($P < 0.001$ and $P = 0.021$ for PDAC and NSCLC, respectively; Figure 2F, G).

Collectively, these findings indicate that CLIC1 is upregulated in HCC, and its upregulation is associated with tumor invasion and metastasis and poor clinical outcomes.

CLIC1 facilitates adherence and extravasation of tumor cells for metastasis in mice. To verify the clinical findings that CLIC1 facilitates tumor invasion and metastasis, we used xenograft tumor assays in mice. We first examined CLIC1 expression in a panel of hepatoma cell lines. Cells with high CLIC1 expression displayed relatively mesenchymal traits and high invasiveness (SK-Hep1 and Mahlavu cells vs. Hep3B and HepG2 cells; supplemental Figure 2). We then silenced CLIC1 expression by using siRNAs (siCLIC1) or small hairpin RNAs (shCLIC1) in luciferase-transformed SK-Hep1 and Huh7 cells for xenograft tumor metastasis in nude mice. Lung metastasis assays were performed by injection of tumor cells through the tail veins of nude mice. Four hours after the injection, approximately equal amounts of tumor cells targeted to the lungs in all four groups were observed (Figure 3A). However, 5-9 weeks after the injection, overt lung metastasis developed in the control groups (siNC, siRNAs containing scrambled sequences; or shEV, shRNA harboring empty vector), but relatively low (siCLIC1) or undetectable signals (shCLIC1) of lung metastasis were found when CLIC1 was transiently (siCLIC1) or constitutively silenced (shCLIC1) (Figure 3A-D). The silencing

efficiency of the inoculated tumor cells was confirmed by immunoblotting assays (Figure 3E). Moreover, constitutively silenced CLIC1 in the xenograft HCC cells prolonged the overall survival of the mice (P = 0.0049, shEV vs. shCLIC1; Figure 3F), while transient silencing of CLIC1 by siCLIC1 exerted only a marginally protective effect (P = 0.083; Figure 3G).

Consistently, CLIC1 depletion (shCLIC1) suppressed liver metastasis (as compared to the control, shEV), which was performed by injection of Huh7 cells through the spleen into nude mice (Figure 3H-K).

In tail-vein injection mouse models, lung metastasis involves 1) adherence in the lung/extravasation, 2) pre-metastatic niche formation, and 3) colonization/proliferation of tumor cells in the metastatic cascade (30). To identify which steps of metastasis was inhibited by CLIC1 depletion, we did lung dissection at different time points after injection of the GFP (green-fluorescence protein)-labeled tumor cells through tail vein in nude mice. As shown in Figure 3L, equal numbers of tumor cells with (shCLIC1) and without (shEV) CLIC1 depletion were detected in the lung sections at 4 and 8 h, followed by a rapid loss of the shCLIC1-tumor cells, but not shEV-cells, in the lung tissue at 12 h and after that. This finding suggested a defect in the adherence in the lung alveoli and extravasation steps rather than in the subsequent colonization of tumor cells in the lung metastasis cascade.

To further verify the hypothesis, we seeded SK-Hep1 and Mahlavu cells with and without CLIC depletion on the laminin-coated plates. Cells with CLIC1 depletion significantly lost their adhesion to

157 the plats as compared to the control ($P < 0.001$ for both SK-Hep1 and Mahlavu cells; Figure 3M).
158 Therefore, CLIC1 is critically required for tumor cells adhering to the extracellular matrix.
159 Together, our findings suggest that CLIC1 plays a pivotal role in the adherence and
160 extravasation of tumor cells in the metastasis cascade.
161
162 *CLIC1 facilitates filopodia, lamellipodia, and invadopodia upon migration induction.* Given that
163 adhesion to the extracellular matrix and membranous protrusions are the fundamental processes
164 for cell migration and tumor invasion and metastasis, we evaluated the roles of CLIC1 in the
165 formation of membrane protrusions. We examined the roles of CLIC1 in cell migration and invasion
166 in vitro. Transwell assays showed that CLIC1 depletion (shCLIC1) significantly suppressed the
167 migration and invasion (with and without Matrigel coating, respectively) of SK-Hep1, Mahlavu, and
168 Huh7 cells (Figure 4,A and B). In contrast, ectopic expression of CLIC1 in Huh7, HepG2, and Tong
169 cells (poorly motile cells) enhanced their migration and invasion (Figure 4, C and D; Supplemental
170 Figure 3, A and B). The silencing and induction efficiencies of CLIC1 expression are summarized in
171 Supplemental Figure -3C.
172 Notably, CLIC1 depletion in SK-Hep1, Mahlavu, Hep3B, and Huh7 cells or ectopic expression of
173 CLIC1 in Huh7 and HepG2 cells did not affect cell proliferation (Supplemental Figure 4). Thus, CLIC1
174 is functionally involved in the regulation of tumor cell migration and invasion in vitro and tumor
175 metastasis in vivo.

We then studied the role of CLIC1 in membrane protrusion in response to migration-related stimuli. We cocultured Huh7 cells with and without CLIC1 silencing on the same plate. As shown in Figure 4E, free-space exposure induced the formation of filopodia in control cells, but not in the cells with CLIC depletion (negative for green fluorescence, Figure 4E; P = 0.032). Interestingly, some CLIC1 was targeted to the tip of filopodia. In response to epithelial growth factor (EGF) treatment (chemotaxis), the formation of lamellipodia was induced in the control cells (shEV), but not in cells with CLIC1 depletion (shCLIC1, Figure 4F). Notably, CLIC1 accumulated at the leading edge of lamellipodia was seen (Figure 4F, rightmost panel). In a time-lapse observation for cell response to EGF treatment, CLIC1-GFP (fusion with green fluorescence protein) and GFP were initially evenly distributed in the cytosol with spared membrane edges (Figure 4G, 0 sec). Then, some CLIC1-GFP, but not GFP, was targeted to the leading edge of the membrane protrusions of migrating cells (Figure 4G). In three-dimensional invasion assays, CLIC1 was targeted to the front end of invading tumor cells (Figure 4H), while the invasion was suppressed in the tumor cells with CLIC1 depletion (Figure 4B). Therefore, these findings suggest CLIC1 is targeted to the tips of the membrane protrusions, and plays a crucial role in the formation of filopodia, lamellipodia, and invadopodia for cell migration and tumor invasion.

CLIC1 directs the formation of nascent cell-matrix adhesions and signaling. Since cell-matrix adhesions are the membranous hubs essential for cell adhering to the extracellular matrix and

195 migration, we speculated that CLIC1 might be involved in the formation of nascent cell-matrix
196 adhesions. We examined the formation of cell-matrix adhesions in response to EGF (chemotaxis;
197 Figure 5A) and exposure to free space (wounding, mechanotaxis; Figure 5B). The results showed
198 that CLIC1 was not only targeted to the leading edge plasma membrane but also colocalized with
199 vinculin and talin (Figure 5A, B, white arrowheads), landmarks of cell-matrix adhesions. In contrast,
200 the lamellipodia formation was substantially suppressed in cells with CLIC1 depletion (Figure 5A, B,
201 open arrowheads). To further confirm that CLIC1 was targeted to nascent cell-matrix adhesions, we
202 inspected the formation of nascent cell-matrix adhesions by reseeding CLIC1-GFP transfected cells
203 on culture plates. CLIC1 was translocated to the membranous margin 15 min after reseeding and
204 then transiently targeted to the edge of membrane protrusions morphologically consistent with
205 nascent cell-matrix adhesions (30 m, Supplemental Figure 5A). We then cotransfected cells with
206 CLIC1-RFP (red-fluorescence protein) and GFP-tagged adhesion marks, including talin, vinculin, and
207 paxillin (Figure 5C). The membranous CLIC1 was colocalized with talin, vinculin, and paxillin at the
208 nascent adhesions (Figure 5C, right panel).

209 In contrast, neither the membrane domain-deleted mutant CLIC1 (dCLIC1-GFP, deletion of aa 2-
210 90) nor GFP was targeted to the nascent cell-matrix adhesions (Figure 5D). Moreover, the formation
211 of nascent cell-matrix adhesions was also decreased in cells with CLIC1 depletion (Figure 5A, B).
212 These findings suggested that CLIC1 is required for the assembly of nascent cell-matrix adhesions,
213 which is dependent on the membrane-associated domain of CLIC1.

214 To further verify the role of CLIC1 in the assembly of nascent cell-matrix adhesions, we used
215 co-immunoprecipitation assays to inspect the integrity of cell-matrix adhesions between the cells
216 with and without CLIC1 depletion. We found that CLIC1 depletion slightly decreased the levels of
217 talin, vinculin, and Src, but not β-actin, FAK, or caveolin1 (Figure 5E). However, the silencing of CLIC1
218 decreased the vinculin, FAK, Src, β-actin, and caveolin levels in the precipitate by using anti-talin
219 antibodies (Figure 5F, left panel); decreased the vinculin, Src, and β-actin levels in the precipitate by
220 using anti-FAK (Figure 5F, middle panel); decreased the FAK and β-actin levels in the precipitate by
221 using anti-Src (Figure 5F, right panel); and reduced the vinculin, FAK and Src levels in the precipitate
222 by using anti-β-actin (Supplemental Figure 5B). The results are summarized in Figure 5G.
223 Collectively, silenced CLIC1 expression disrupts the integrity of cell-matrix adhesions. Indeed, as
224 shown in Figure 5A, B, in CLIC1-depleted cells, the formation of nascent cell-matrix adhesions at the
225 leading edge of migrating cells was substantially suppressed (open arrowheads indicate cells with
226 CLIC1 depletion and no nascent adhesion formed).
227 If CLIC1 facilitates the assembly of nascent cell-matrix adhesions, we predicted that CLIC1
228 promotes the nascent adhesion-mediated signaling. We compared adhesion-mediated cellular
229 signaling between inactive (no nascent adhesion formatin) or reseeded (inducing nascent
230 adhesions) cells. We found that CLIC1 depletion only suppressed the phosphorylation of FAK, Src,
231 and AKT in reseeded cells but not in inactive cells (Figure 5H, left panel). Moreover, CLIC1 depletion
232 selectively suppressed the ITGB4 and ITGA4 levels as well as the phosphorylation of Src and AKT in

233 the reseeded cells but not in inactive cells (Figure 5H, right panel), suggesting that CLIC1 is
234 selectively involved in the regulation of nascent, but not mature, adhesion-mediated signaling.
235 Overall, these findings support the hypothesis that CLIC1 is specifically required for the
236 induction of nascent cell-matrix adhesions and signaling, which is known to drive F-actin elongation
237 for lamellipodia and filopodia formation (31).
238
239 *CLIC1 recruits PIP5K to the plasma membrane to initiate "PIP_2-talin-integrin"-mediated cell-*
240 *matrix adhesion formation.* To further investigate the mechanism by which CLIC1 facilitates nascent
241 adhesion formation, we used IP and found the PIP5K1A and PIP5K1C were bound to CLIC1 (Figure
242 6A, C). Specific binding of PIP5K1A and PIP5K1C with CLIC1 was further confirmed by reciprocal IP
243 assays (Figure 6B) or competition binding assays with a recombinant CLIC1 (Figure 6D).
244 We then inspected the interaction of PIP5K1A and PIP5K1C with CLIC1 at the subcellular level.
245 We found that EGF induced co-targeting of CLIC1 and PIP5K1A to the leading edge of membrane
246 protrusions (Figure 6E). Consistently, free-space exposure induced co-targeting of CLIC1 and
247 PIP5K1A to the leading edge of lamellipodia in two primary HCC cell lines derived from patients of
248 HCC (Supplemental Figure 6). However, in response to EGF treatment, not only the membrane-
249 targeting of PIP5K1A but also the formation of membrane protrusions were substantially reduced in
250 the cells with CLIC1 depletion (Figure 6F; open arrowheads) as compared with cells without CLIC1
251 deletion (Figure 6F; arrowheads). Consistently, CLIC1 depletion suppressed accumulation of PIP5K1C

252 to the plasma membrane and colocalization with nascent cell-matrix adhesions in reseeding assays
253 [red arrowheads (shCLIC1) vs. yellow arrowheads (shEV); Figure 6G].

254 To further confirm that CLIC1 is required for translocation of PIP5K1A/C from the cytosol to the
255 plasma membrane, we compared the PIP5K1A levels associated with the plasma membrane and in
256 the cytosol in response to EGF treatment. EGF treatment increased the membranous PIP5K1A by
257 2.5 folds, but not the cytosolic PIP5K1A, in cells without CLIC1 depletion, consistent with membrane
258 translocation of PIP5KIA (Figure 6H, lane 1,2, 5, 6). However, in cells with CLIC1 depletion, not only
259 the membranous PIP5K1A level was substantially decreased but also the response to EGF treatment
260 was abolished (Figure 6H, lane 3, 4). Therefore, CLIC1 is required for the recruitment of PIP5K1A to
261 membrane. As a result, our data support the hypothesis that, in response to chemotaxis or
262 mechanotaxis (free-space exposure), the membrane-targeted CLIC1 recruits PIP5K1A/C to the
263 plasma membrane to facilitate the formation of nascent cell-matrix adhesions.

264 It is known that talin can be activated by phosphatidylinositol 4,5-bisphosphate (PIP_2), which is
265 a product of PIP5Ks, resulting in the assembly of integrin-mediated adhesions (32, 33). We thus
266 tested whether the membrane-targeting of CLIC1 facilitated PIP_2 accumulation in the plasma
267 membrane for nascent cell-matrix adhesions. As shown in Figure 6I, in the reseeded cells, PIP_2 was
268 highly accumulated at the edge of the plasma membrane (left panel) where nascent cell-matrix
269 adhesions were formed. In contrast, CLIC1 depletion suppressed the accumulation of PIP_2 in the
270 plasma membrane (right panel).

271 Collectively, the above findings support the hypothesis that CLIC1 recruits PIP5Ks to the plasma
272 membrane to activate the PIP5K-PIP_2-talin-integrin signaling pathway to induce nascent adhesions
273 and adhesion-mediated signals. As such, ectopic expression or activation of PIP5Ks or talin would
274 restore the nascent adhesion formation and signals in the cells with CLIC1 depletion. Consistently,
275 ectopic expression of PIP5K1C or talin prevented the suppression of nascent adhesion-mediated
276 signaling (phosphorylation of FAK, Paxillin, and Src) and integrins-α4 and -β4 by CLIC1 depletion
277 (Figure 6, J-L).
278
279 *The expression levels of adhesion-related effectors predict poor clinical outcomes in HCC.*
280 Given that cell-matrix adhesions play a crucial role in tumor invasion and metastasis, we
281 hypothesized that the cell-matric adhesion markers might predict clinical outcomes as does CLIC1 in
282 patients of HCC. We retrieved a cohort of 370 HCC patients from TCGA database (34). We found a
283 positive correlation of the CLIC1 expression levels with the cell-matrix adhesion markers, including
284 talin (P = 5.6e-10; R=0.32), vinculin (P = 2.2e-12; R=0.35), paxillin (P = 0; R=0.49), and FAK (P = 2.8e-
285 11; R=0.34; Figure 7A). Interestingly, high expression levels of talin (HR = 1.44; P = 0.039), vinculin
286 (HR = 1.74; P = 0.0027), paxillin (HR = 1.79; P = 0.0017), and FAK (PTK2; HR = 1.49; P = 0.030) in HCC
287 were associated with a high mortality rate (Figure 7B). These findings further support the
288 implication of cell-matrix adhesions in HCC progression.
289
290 *CLIC1 and its ion conductance are therapeutic targets for tumor metastasis.* Given that

291 membranous CLIC1 can function as a chloride ion channel (17, 20, 35) and is associated with tumor
292 invasion and metastasis, we speculate that CLIC1 or its chloride conductance are potential
293 therappeutic targets for tumor metastasis. To test this hypothesis, we treated tumor cells with
294 indanyloxyacetic (IAA)-94, a small molecule that is known to inhibit CLIC family channel (35, 36). We
295 found that IAA-94 interfered with tumor-cell adhesion to the laminin-coated culture plates
296 compared to what treated with dimethyl sulfoxide (DMSO, the solvent) as a control (Figure 8A),
297 similar to the suppression of cell adhesion by CLIC1 depletion (Figure 3M). We then injected
298 luciferase-transduced SK-Hep1 cells through tail veins of nude mice to assay lung metastasis. As
299 shown in Figure 8B, equal numbers of tumor cells were trapped in the lungs 3 h after injection.
300 However, IAA-94 treatment or constitutive silencing of CLIC1 significantly suppressed the
301 subsequent lung metastasis (50 d after injection; $P < 0.001$, shEV vs. shCLIC1; $P < 0.001$, DMSO vs.
302 IAA-94). We dissected lung tissues (Figure 8C) and confirmed the suppression of lung metastasis
303 either by silencing CLIC1 expression with shRNAs (17.4 vs. 0 per-lung, $P < 0.001$) or IAA-94
304 treatment (19.8 vs. 0 per-lung, $P < 0.001$, Figure 8C, right panel).

305 Overall, our study supports the hypothesis that in response to chemotactic or mechanotactic
306 stimuli, CLIC1 recruits PIP5K1A/C to the leading edge of the plasma membrane, where PIP5K1A/C
307 generate a PIP_2-rich microdomain to activate talin (37, 38). The activated talin then induces the
308 formation of integrin-mediated adhesions and signals for lamellipodia/invadopodia formation in a
309 spatiotemporal regulatory manner (Figure 8D). Aberrant CLIC1 upregulation, which is frequently

found in metastatic tumors, endows tumor cells with high motility and invasiveness. Inhibition of CLIC1 or its ion conductance are promising approaches for the prevention and treatment of tumor invasion and metastasis.

Discussion

Efficient membrane protrusion and adhering to the extracellular matrix are fundamental cell processes and crucial for migration, in particular, in tumor invasion and metastasis. In this study, we identified CLIC1 that is upregulated in human HCC and associated with tumor invasion, metastasis, and poor clinical outcomes. We further demonstrated that, in response to chemotaxis and mechanotaxis, CLIC1 is targeted from the cytosol to the leading edge of the plasma membrane to form both nascent cell-matrix adhesions and the signals for lamellipodia and invadopodia formation in a spatiotemporal regulatory manner. Our findings provide a clue to the answer to a long-term enigma of how tumor cells efficiently regulate lamellipodia and invadopodia for invasion and metastasis.

CLIC1 shuttles between the cytosol and plasma membrane through conformational changes (17) without known biological significance (39). We herein report that in response to chemotaxis by EGF or mechanotaxis by disrupting cell-cell contacts (temporal factors), PIP5K1A/C are recruited by CLIC1 to the leading edge of the plasma membrane, where PIP5K1A/C generate a PIP2-rich

329 microdomain (spatial factors). It is known that PIP_2 clusters activate talin by way of a “pull-push”
330 mechanism (38), resulting in inducing integrin-mediated cell-matrix adhesion formation (37, 40).
331 Therefore, the shuttling of CLIC1 between the cytosol and plasma membrane spatiotemporally
332 regulates the formation of filopodia, lamellipodia, and invadopodia for directional cell migration and
333 tumor invasion and metastasis.

334 The ability of CLIC1 to shuttle between the cytosol and plasma membrane and its involvement
335 in the regulation of cell adhesion to the extracellular matrix are reminiscent of those found for
336 other CLIC-family members. Argenzio et al. found that CLIC4 is rapidly recruited to the plasma
337 membrane and colocalized with β1 integrin in response to the activation of RhoA-mediated
338 signaling (41, 42). Moreover, CLIC4 is critical for β1 integrin internalization and recycling.
339 Interestingly, the membrane-targeting of CLIC4 provides a feedback mechanism to counteract
340 filopodium formation (41). CLIC3 is upregulated and required for the invasion of breast and
341 pancreatic cancers by regulating Rab25-dependent $\alpha5\beta1$ integrin recycling (43) and Rab25-
342 independent MMP14 recycling (44). Apparently, different CLIC members have different cellular
343 functions but share similar molecular mechanisms.

344 Since CLIC1 is upregulated in many types of human cancers and selectively targeted to the
345 plasma membrane in tumor cells, it can be a promising target for the anticancer treatment of
346 invasion and metastasis. Notably, the *CLIC1* gene is highly conserved among tumors with only 2% of
347 patients harboring missense or nonsense mutations, indicating that its role in tumorigenesis is more

348 related to its membrane localization-associated activity than to mutations (45). Gurski et al.
349 reported that in renal cell carcinoma, CLIC1 cooperates with integrin αvβ3 and fibronectin to
350 stabilize invadopodia for tumor invasion by regulating myosin light chain kinase (MYLK) (46).
351 Recently, it was reported that silencing CLIC1 impairs the proliferative capacity and self-renewal
352 properties of glioblastoma cells, thereby indicating the vital role of CLIC1 in sustaining the stemness
353 of cancer cells. Given that cancer cells with cheom-resistance and metastasis have been attributed
354 to a minor fraction of tumors with stemness properties, targeting CLIC1 provides a novel approach
355 to directly eradicate such cancer stem cells (47, 48). Further studies to evaluate the efficacy of anti-
356 cancer therapy by targeting CLIC1 in human cancers are warranted.

357 In summary, membrane targeting of CLIC1 regulates nascent cell–matrix adhesions, signaling,
358 and membrane protrusions by way of transporting PIP5Ks to the plasma membrane. This CLIC1-
359 PIP5K-PIP_2-talin-integrins-adhesions signaling pathway orchestrates the spatiotemporal formation
360 of lamellipodia and invadopodia for tumor invasion and metastasis. Our findings suggest that CLIC1,
361 with its unique properties in cancer cells, can serve as an excellent target for the prevention and
362 treatment of invasion and metastasis in cancers.

363

364 ## Methods

365 *Cell lines, cDNA clones, siRNAs, shRNAs, and reagents.* We used Huh7, Hep3B, Mahlavu, and
366 HepG2 (human hepatoma cell lines), SK-Hep1 (a human hepatic adenocarcinoma cell line), and two

367 primary HCC cell lines, LT87 and PDX57, which were derived from two patients with HCC in this study.
368 For immunoprecipitation assays, we used human 293T cells because of their high efficiency in the
369 expression of transduced clones. The cells were cultured in DMEM (ThermoFisher Scientific,
370 Massachusetts, USA) with 10% FBS. The plasmids, pCLIC1-GFP was from Origene (#RG218042), and
371 pPIP5K1A-Myc (the PIP5K1A cDNA was from Addgene, #20580, which was cloned into pCMV6-Myc),
372 pPIP5K1C-GFP (pEGFP-C2-PIP5K1C90 was from Addgene (#22299), and PLC-delta-GFP were from
373 Addgene (#21179). The target sequences of siRNA or shRNA for CLIC1 were (1)
374 TGGCTCAAGGAGTCACCTTCAATG; and (2) CCCATTCCTGCTGTATGGCACTGAA (Thermo Fisher Scientific).
375 The MQAE staining reagent was from Thermo Fisher (catalog number: E3101). R(+)-IAA-94 was
376 purchased from Sigma (catalog number: I117). Pseudolentivirus for shRNAs targeting CLIC1 mRNA
377 (shCLIC1), luciferase (shLuc), or an empty vector (shEV) were obtained from National RNAi Core,
378 Taiwan. Overexpression of CLIC1 was performed using the Lenti-X^{TM} Tet-Off$^{®}$ Advanced Inducible
379 expression system (632163; Clontech) according to the manufacturer's instructions.

380 *Comparative Proteomics.* For two-D proteomics, we collected tumor and para-tumor liver tissues
381 from seven patients of hepatic focal nodular hyperplasia, 12 cases of early HCC (solitary tumor < 3 cm
382 without vascular invasion), and 13 cases of invasive HCC (with invasion into main branches of the
383 portal or hepatic veins), who received hepatectomy in our hospital. Two-D gel electrophoresis, gel
384 staining, image analysis, and protein identification were performed as previously described (49).

385 *In vivo metastasis assays.* We used SK-Hep1 and Huh7 cells for in vivo metastasis assays,

386 including lung metastasis via tail vein injection and liver metastasis via spleen injection, as previously
387 described (29). We transduced SK-Hep1 and Huh7 cells with the lentivirus vector carrying a dual
388 GFP/luciferase expression system (SK-Hep1-GL and Huh7-GL cells). We then transduced SK-Hep1-GL
389 Huh7 cells with shEV or shCLIC1 and with siRNAs targeting CLIC1 (siCLIC1) or scrambled sequences
390 (siNC). We injected 1 x 10^6 SK-Hep1 cells in 200 μL PBS per mouse into BALB/c null mice
391 (BALB/cAnN.Cg-*Foxn1*^{nu}/CrlNarl) through the tail veins or 5 x 10^5 Huh7 cells in 100 μL PBS per mouse
392 spleen for lung and liver metastasis, respectively. To compare the effect of IAA-94 treatment on
393 tumor metastasis, mice were intraperitoneally injected with DMSO or IAA-94 (50 mg/kg of body
394 weight). We used the IVIS image analysis system (to monitor the location and relative amounts of
395 these transduced cells in mice at the indicated time points. Quantitative analysis of lung or liver
396 metastasis was performed by using software (Living Image 4.0, PerkinElmer). The lung or liver sections
397 were taken, followed by the analysis of fluorescence-positive cells to determine xenograft-tumor
398 invasion and metastasis.

399 *Immunofluorescence staining.* We conducted immunofluorescence staining to track the
400 expression and subcellular location of the indicated proteins, as described previously (50). In brief,
401 we first fixed cells in 4% paraformaldehyde, permeabilized the plasma membrane in 0.1% Triton X-
402 100, blocked the background signals with a buffer containing 1% BSA, 0.1% Tween-20 for 30 min,
403 treated the cells with primary antibodies (talin, vinculin, paxillin, FAK, PIP5K1A; 1:200) overnight at
404 4°C, washed the samples with PBST three times, and then added secondary antibodies (phalloidin-

405 Alexa488 or -Alexa594; 1:200 in blocking buffer) for 30 min. We counterstained the nuclei with DAPI
406 for 5 min and mounted the samples with Prolong Gold antifade reagent. We inspected and analyzed
407 the results using a confocal microscope (SP8, Leica) and Leica Application Suite Core X software
408 (version 3.3.0).

409 *Detection of PI(4, 5)P2.* We determined the amount of PI(4, 5)P2 by transfecting cells with a GFP-
410 plasmid to express PLCdelta, which contains the PI(4, 5)P2 lipid selective PH domain as a fluorescent
411 translocation biosensor to determine the concentration of PI(4, 5)P2 lipids (51). Fluorescence
412 intensity and quantification were analyzed by ImageJ software (version 1.43).

413 *Time-lapse imaging.* We labeled the target proteins with GFP or RFP. We trypsinized and
414 reseeded cells onto a dish coated with fibronectin (10 ng/mL). Cells with fluorescence-tagged
415 proteins were monitored by using a Leica SP8 inverted microscope with an enclosed incubator (5%
416 CO_2, 374°C). The intensity and performance of the fluorescence were analyzed by Leica Application
417 Suit Core X software (version 3.3.0).

418 *Wound healing assay, transwell migration, and invasion assay.* We assayed cell migration and
419 invasion with previously published protocols (52).

420 *Immunoprecipitation.* We conducted immunoprecipitation using previously published protocols
421 (53). In brief, SK-Hep1-shEV and SK-Hep1-shCLIC1 cells were cultured in DMEE with 10% FBS and
422 harvested for IP as growing up to 80% confluence. After being washed cells were lysed in a buffer
423 containing 50 mM Tris (pH 8.0), 150 mM NaCl, 1% Triton X-100, and protease and phosphatase

424 inhibitors (Roche) for 15 min. Cell debris was removed by centrifugation at 12k rpm at 4°C for 15
425 min. An equal amount of protein (1 mg) was subjected to immunoprecipitation with the
426 corresponding primary antibodies and Protein G Mag Sepharose Xtra (Blossom Biotechnologies, Inc.)
427 according to the manufacturer's instructions. Nonimmune IgG or Protein G-Sepharose beads were
428 used as negative controls.

429 *TCGA human HCC cohorts and data processing.* An HCC cohort was containing 370 cases,
430 including 168, 84, 82, and 6 at tumor stage I, II, III, and IV, respectively, were retrieved from The Cancer
431 Genome Atlas (TCGA) databases queried by CLIC1, HCC, survival rate, and gene expression as
432 keywords. The expression of CLIC1 in patients was sorted, and survival plots were analyzed by using
433 the UCSC Xena Functional Genomics Explorer (https://xenabrowser.net) and SurvExpress
434 (http://bioinformatica.mty.itesm.mx:8080/Biomatec/SurvivaX.jsp). The cumulative survival curves
435 for talin, vinculin, paxillin, and FAK were performed by using the software of Kaplan-Meier Plotter
436 (https://kmplot.com/analysis/index.php?p=service) (34).

437 *Patients, tissue arrays, immunohistochemistry.* Human HCC tissue arrays containing 45 cases of
438 chronic hepatitis B- and 45 cases of chronic hepatitis C-associated HCC were obtained from the Taiwan
439 Liver Cancer Network (53). These patients underwent hepatectomy in 2008 in our hospital. The
440 average follow-up time for these patients was 41 months (ranging from 2 to 106 months)(53). The
441 immunohistochemistry (IHC) scores [(= the percentage of positive cells $\times$ IHC intensity (0-3)] were
442 determined by using an automation system, inForm® Advanced Image Analysis Software (version 2.3,

PerkinElmer, MA).

Comparative Proteomics. For two-D proteomics, we collected tumor and para-tumor liver tissues from seven patients of hepatic focal nodular hyperplasia, 12 cases of early HCC (solitary tumor < 3 cm without vascular invasion), and 13 cases of invasive HCC (with invasion into main branches of the portal or hepatic veins), who received hepatectomy in our hospital. Two-D gel electrophoresis, gel staining, image analysis, and protein identification were performed as previously described (49).

Statistics. Statistical analyses were performed using GraphPad Prism 8 (GraphPad Software). A Student's *t*-test (2 tailed), Mann-Whitney *U* test, or 1-way or 2-way ANOVA with Dunnett's or Tukey's multiple comparisons test was performed. One-way ANOVA with Dunnett's multiple comparisons test was used for comparisons with the control group, one-way ANOVA with Tukey's multiple comparisons test was used for comparisons between groups and two-way ANOVA with Tukey's multiple comparisons test was used for pairwise comparisons. Unless otherwise noted, all in vitro experiments were performed in at least two independent times, and values represent the mean ± SD. P values less than 0.05 were considered significant.

Study approval. The Internal Review Board approved specimen collection procedures for HCC for the Medical Ethics of Chang Gung Memorial Hospital (201700344A3). All experimental procedures involving mice were approved by the Animal Care and Use Committee of Chang Gung Memorial Hospital (Taiwan) and developed by the Guide for the Care and Use of Laboratory Animals (National Academy of Sciences, USA, 1985).

462

463 **Author contributions**

464 S.Y.H. conceived the concept, designed the studies, and secured funding. J.M.P. and S.H.L.
465 performed the experiments, acquired data, and analyzed data. M.C.Y. collected the clinical samples
466 and data. S.Y.H. and J.M.P. wrote the manuscript. J.M.P. and S.H.L. contributed equally to this
467 study.

468

469 **Acknowledgments**

470 We are grateful to Professor Pien-Chien Huang at Johns Hopkins University for critical review of
471 this manuscript. We thank Miss Hsiao-Ling Huang for excellent assistance, Dr. Donia Alson for
472 English review, and the Microscopy Core, Center for Advanced Molecular Imaging, Laboratory
473 Animal Center, and Clinical Proteomics Core of the Chang Gung Memorial Hospital for their
474 technical assistance, the Taiwan Liver Cancer Network for the HCC tissue arrays, and the National
475 RNAi Core of Taiwan for the lentivirus-based shRNA clones. This work was supported by research
476 grants from the Chang Gung Medical Foundation (CMRPG3F0031-3), National Health Research
477 Institute (NHRI-EX106-10408BI, NHRI-EX109-10806BI), and Ministry of Science and Technology
478 (MOST103-2314-B-182A-117-MY3; MOST107-2314-B-182A-020-MY3), Taiwan.

479

480 **References**

481 1. Yamada KM, and Mayor R. Editorial overview: Cell dynamics in development, tissue

remodelling, and cancer. *Current opinion in cell biology.* 2016;42:iv-vi.

2. Pandya P, Orgaz JL, and Sanz-Moreno V. Modes of invasion during tumour dissemination. *Molecular oncology.* 2017;11(1):5-27.
3. Humphries JD, Chastney MR, Askari JA, and Humphries MJ. Signal transduction via integrin adhesion complexes. *Current opinion in cell biology.* 2019;56:14-21.
4. Lo SH, and Chen LB. Focal adhesion as a signal transduction organelle. *Cancer metastasis reviews.* 1994;13(1):9-24.
5. Calderwood DA, Campbell ID, and Critchley DR. Talins and kindlins: partners in integrin-mediated adhesion. *Nature reviews Molecular cell biology.* 2013;14(8):503-17.
6. Kim C, Ye F, and Ginsberg MH. Regulation of integrin activation. *Annual review of cell and developmental biology.* 2011;27:321-45.
7. Ye F, Lagarrigue F, and Ginsberg MH. SnapShot: talin and the modular nature of the integrin adhesome. *Cell.* 2014;156(6):1340-.e1.
8. Goult BT, Yan J, and Schwartz MA. Talin as a mechanosensitive signaling hub. *The Journal of cell biology.* 2018;217(11):3776-84.
9. Iwamoto DV, and Calderwood DA. Regulation of integrin-mediated adhesions. *Current opinion in cell biology.* 2015;36:41-7.
10. Warner H, Wilson BJ, and Caswell PT. Control of adhesion and protrusion in cell migration by Rho GTPases. *Current opinion in cell biology.* 2019;56:64-70.
11. Lo SH. C-terminal tensin-like (CTEN): a promising biomarker and target for cancer. *The international journal of biochemistry & cell biology.* 2014;51:150-4.
12. Strilic B, and Offermanns S. Intravascular Survival and Extravasation of Tumor Cells. *Cancer cell.* 2017;32(3):282-93.
13. Singh H, Cousin MA, and Ashley RH. Functional reconstitution of mammalian 'chloride intracellular channels' CLIC1, CLIC4 and CLIC5 reveals differential regulation by cytoskeletal actin. *The FEBS journal.* 2007;274(24):6306-16.
14. Goodchild SC, Howell MW, Cordina NM, Littler DR, Breit SN, Curmi PM, et al. Oxidation promotes insertion of the CLIC1 chloride intracellular channel into the membrane. *European biophysics journal : EBJ.* 2009;39(1):129-38.
15. Ulmasov B, Bruno J, Oshima K, Cheng YW, Holly SP, Parise LV, et al. CLIC1 null mice demonstrate a role for CLIC1 in macrophage superoxide production and tissue injury. *Physiological reports.* 2017;5(5).
16. Ulmasov B, Bruno J, Woost PG, and Edwards JC. Tissue and subcellular distribution of CLIC1. *BMC cell biology.* 2007;8:8.
17. Hare JE, Goodchild SC, Breit SN, Curmi PM, and Brown LJ. Interaction of Human Chloride Intracellular Channel Protein 1 (CLIC1) with Lipid Bilayers: A Fluorescence Study. *Biochemistry.* 2016;55(27):3825-33.
18. Singh H, and Ashley RH. Redox regulation of CLIC1 by cysteine residues associated with the

putative channel pore. *Biophysical journal.* 2006;90(5):1628-38.
19. Peter B, Fanucchi S, and Dirr HW. A conserved cationic motif enhances membrane binding and insertion of the chloride intracellular channel protein 1 transmembrane domain. *European biophysics journal : EBJ.* 2014;43(8-9):405-14.
20. Liu B, Billington CK, Henry AP, Bhaker SK, Kheirallah AK, Swan C, et al. Chloride intracellular channel 1 (CLIC1) contributes to modulation of cyclic AMP-activated whole-cell chloride currents in human bronchial epithelial cells. *Physiological reports.* 2018;6(2).
21. Jia N, Dong S, Zhao G, Gao H, Li X, and Zhang H. CLIC1 overexpression is associated with poor prognosis in pancreatic ductal adenocarcinomas. *Journal of cancer research and therapeutics.* 2016;12(2):892-6.
22. Zhang S, Wang XM, Yin ZY, Zhao WX, Zhou JY, Zhao BX, et al. Chloride intracellular channel 1 is overexpression in hepatic tumor and correlates with a poor prognosis. *APMIS : acta pathologica, microbiologica, et immunologica Scandinavica.* 2013;121(11):1047-53.
23. Wang JW, Peng SY, Li JT, Wang Y, Zhang ZP, Cheng Y, et al. Identification of metastasis-associated proteins involved in gallbladder carcinoma metastasis by proteomic analysis and functional exploration of chloride intracellular channel 1. *Cancer letters.* 2009;281(1):71-81.
24. Petrova DT, Asif AR, Armstrong VW, Dimova I, Toshev S, Yaramov N, et al. Expression of chloride intracellular channel protein 1 (CLIC1) and tumor protein D52 (TPD52) as potential biomarkers for colorectal cancer. *Clinical biochemistry.* 2008;41(14-15):1224-36.
25. Chen CD, Wang CS, Huang YH, Chien KY, Liang Y, Chen WJ, et al. Overexpression of CLIC1 in human gastric carcinoma and its clinicopathological significance. *Proteomics.* 2007;7(1):155-67.
26. Chang YH, Wu CC, Chang KP, Yu JS, Chang YC, and Liao PC. Cell secretome analysis using hollow fiber culture system leads to the discovery of CLIC1 protein as a novel plasma marker for nasopharyngeal carcinoma. *Journal of proteome research.* 2009;8(12):5465-74.
27. Ding Q, Li M, Wu X, Zhang L, Wu W, Ding Q, et al. CLIC1 overexpression is associated with poor prognosis in gallbladder cancer. *Tumour biology : the journal of the International Society for Oncodevelopmental Biology and Medicine.* 2015;36(1):193-8.
28. Li RK, Zhang J, Zhang YH, Li ML, Wang M, and Tang JW. Chloride intracellular channel 1 is an important factor in the lymphatic metastasis of hepatocarcinoma. *Biomedicine & pharmacotherapy = Biomedecine & pharmacotherapie.* 2012;66(3):167-72.
29. Peng JM, Bera R, Chiou CY, Yu MC, Chen TC, Chen CW, et al. Actin cytoskeleton remodeling drives epithelial-mesenchymal transition for hepatoma invasion and metastasis in mice. *Hepatology (Baltimore, Md).* 2018;67(6):2226-43.
30. Gómez-Cuadrado L, Tracey N, Ma R, Qian B, and Brunton VG. Mouse models of metastasis: progress and prospects. *Disease models & mechanisms.* 2017;10(9):1061-74.
31. Kadry YA, and Calderwood DA. Chapter 22: Structural and signaling functions of integrins. *Biochimica et biophysica acta Biomembranes.* 2020;1862(5):183206.

32. De Craene JO, Bertazzi DL, Bar S, and Friant S. Phosphoinositides, Major Actors in Membrane Trafficking and Lipid Signaling Pathways. *International journal of molecular sciences.* 2017;18(3).
33. Hammond GR. Does PtdIns(4,5)P2 concentrate so it can multi-task? *Biochemical Society transactions.* 2016;44(1):228-33.
34. Menyhárt O, Nagy Á, and Győrffy B. Determining consistent prognostic biomarkers of overall survival and vascular invasion in hepatocellular carcinoma. *Royal Society open science.* 2018;5(12):181006.
35. Edwards JC. The CLIC1 chloride channel is regulated by the cystic fibrosis transmembrane conductance regulator when expressed in Xenopus oocytes. *The Journal of membrane biology.* 2006;213(1):39-46.
36. Skaper SD, Facci L, and Giusti P. Intracellular ion channel CLIC1: involvement in microglia-mediated β-amyloid peptide(1-42) neurotoxicity. *Neurochemical research.* 2013;38(9):1801-8.
37. Orlowski A, Kukkurainen S, Poyry A, Rissanen S, Vattulainen I, Hytonen VP, et al. PIP2 and Talin Join Forces to Activate Integrin. *The journal of physical chemistry B.* 2015;119(38):12381-9.
38. Wang JH. Pull and push: talin activation for integrin signaling. *Cell research.* 2012;22(11):1512-4.
39. Salao K, Jiang L, Li H, Tsai VW, Husaini Y, Curmi PM, et al. CLIC1 regulates dendritic cell antigen processing and presentation by modulating phagosome acidification and proteolysis. *Biology open.* 2016;5(5):620-30.
40. Ye X, McLean MA, and Sligar SG. Conformational equilibrium of talin is regulated by anionic lipids. *Biochimica et biophysica acta.* 2016;1858(8):1833-40.
41. Argenzio E, Klarenbeek J, Kedziora KM, Nahidiazar L, Isogai T, Perrakis A, et al. Profilin binding couples chloride intracellular channel protein CLIC4 to RhoA-mDia2 signaling and filopodium formation. *The Journal of biological chemistry.* 2018;293(50):19161-76.
42. Argenzio E, Margadant C, Leyton-Puig D, Janssen H, Jalink K, Sonnenberg A, et al. CLIC4 regulates cell adhesion and beta1 integrin trafficking. *Journal of cell science.* 2014;127(Pt 24):5189-203.
43. Dozynkiewicz MA, Jamieson NB, Macpherson I, Grindlay J, van den Berghe PV, von Thun A, et al. Rab25 and CLIC3 collaborate to promote integrin recycling from late endosomes/lysosomes and drive cancer progression. *Developmental cell.* 2012;22(1):131-45.
44. Macpherson IR, Rainero E, Mitchell LE, van den Berghe PV, Speirs C, Dozynkiewicz MA, et al. CLIC3 controls recycling of late endosomal MT1-MMP and dictates invasion and metastasis in breast cancer. *Journal of cell science.* 2014;127(Pt 18):3893-901.
45. Barbieri F, Verduci I, Carlini V, Zona G, Pagano A, Mazzanti M, et al. Repurposed Biguanide Drugs in Glioblastoma Exert Antiproliferative Effects via the Inhibition of Intracellular

Chloride Channel 1 Activity. *Frontiers in oncology.* 2019;9:135.

46. Gurski LA, Knowles LM, Basse PH, Maranchie JK, Watkins SC, and Pilch J. Relocation of CLIC1 promotes tumor cell invasion and colonization of fibrin. *Molecular cancer research : MCR.* 2015;13(2):273-80.

47. Setti M, Savalli N, Osti D, Richichi C, Angelini M, Brescia P, et al. Functional role of CLIC1 ion channel in glioblastoma-derived stem/progenitor cells. *Journal of the National Cancer Institute.* 2013;105(21):1644-55.

48. Barbieri F, Wurth R, Pattarozzi A, Verduci I, Mazzola C, Cattaneo MG, et al. Inhibition of Chloride Intracellular Channel 1 (CLIC1) as Biguanide Class-Effect to Impair Human Glioblastoma Stem Cell Viability. *Frontiers in pharmacology.* 2018;9:899.

49. Hsieh SY, Zhuang FH, Wu YT, Chen JK, and Lee YL. Profiling the proteome dynamics during the cell cycle of human hepatoma cells. *Proteomics.* 2008;8(14):2872-84.

50. Lo SJ, Fan LC, Tsai YF, Lin KY, Huang HL, Wang TH, et al. A novel interaction of nucleophosmin with BCL2-associated X protein regulating death evasion and drug sensitivity in human hepatoma cells. *Hepatology (Baltimore, Md).* 2013;57(5):1893-905.

51. Gulshan K, Brubaker G, Conger H, Wang S, Zhang R, Hazen SL, et al. PI(4,5)P2 Is Translocated by ABCA1 to the Cell Surface Where It Mediates Apolipoprotein A1 Binding and Nascent HDL Assembly. *Circulation research.* 2016;119(7):827-38.

52. Peng JM, Bera R, Chiou CY, Yu MC, Chen TC, Chen CW, et al. Actin cytoskeleton remodeling drives epithelial-mesenchymal transition for hepatoma invasion and metastasis. *Hepatology (Baltimore, Md).* 2017.

53. Bera R, Chiou CY, Yu MC, Peng JM, He CR, Hsu CY, et al. Functional genomics identified a novel protein tyrosine phosphatase receptor type F-mediated growth inhibition in hepatocarcinogenesis. *Hepatology (Baltimore, Md).* 2014;59(6):2238-50.

54. Al-Momany A, Li L, Alexander RT, and Ballermann BJ. Clustered PI(4,5)P(2) accumulation and ezrin phosphorylation in response to CLIC5A. *Journal of cell science.* 2014;127(Pt 24):5164-78.

Table 1. Correlation of CLIC1 levels to clinical manifestations in 89 HCC cases

	Group	low CLIC level	high CLIC level	Total	*p*-value	statistical
Gender	Male	31	31	62	0.15	Chi-square
	Female	18	9	27		
Age (y)	20-29	1	0	1	0.563	Kruskal-Wallis
	30-39	1	8	9		
	40-49	21	12	33		
	50-59	17	10	27		
	60-69	8	10	18		
	70-79	1	0	1		
Tumor stage	I	21	9	30	0.006	Kruskal-Wallis
	II	18	12	30		
	IIIB	10	19	29		
Etiology	HBV	24	21	45	0.745	Chi-square
	HCV	25	19	44		
Vascular invasion	0	26	13	39	0.018	Kruskal-Wallis
	1	1	1	2		
	2	19	18	37		
	3-4	3	8	11		

IHC score = percentage of positive cells × IHC intensity (0-3);

High IHC score ≥ 200; low IHC score < 200

HBV: hepatitis B virus; HCV: hepatitis C virus

Vascular invasion grade: 0: no vascular invasion; 1: capsular vein invasion; 2: microscopic vascular invasion; 3: gross vascular invasion; 4: main branches of the portal or hepatic vein invasion

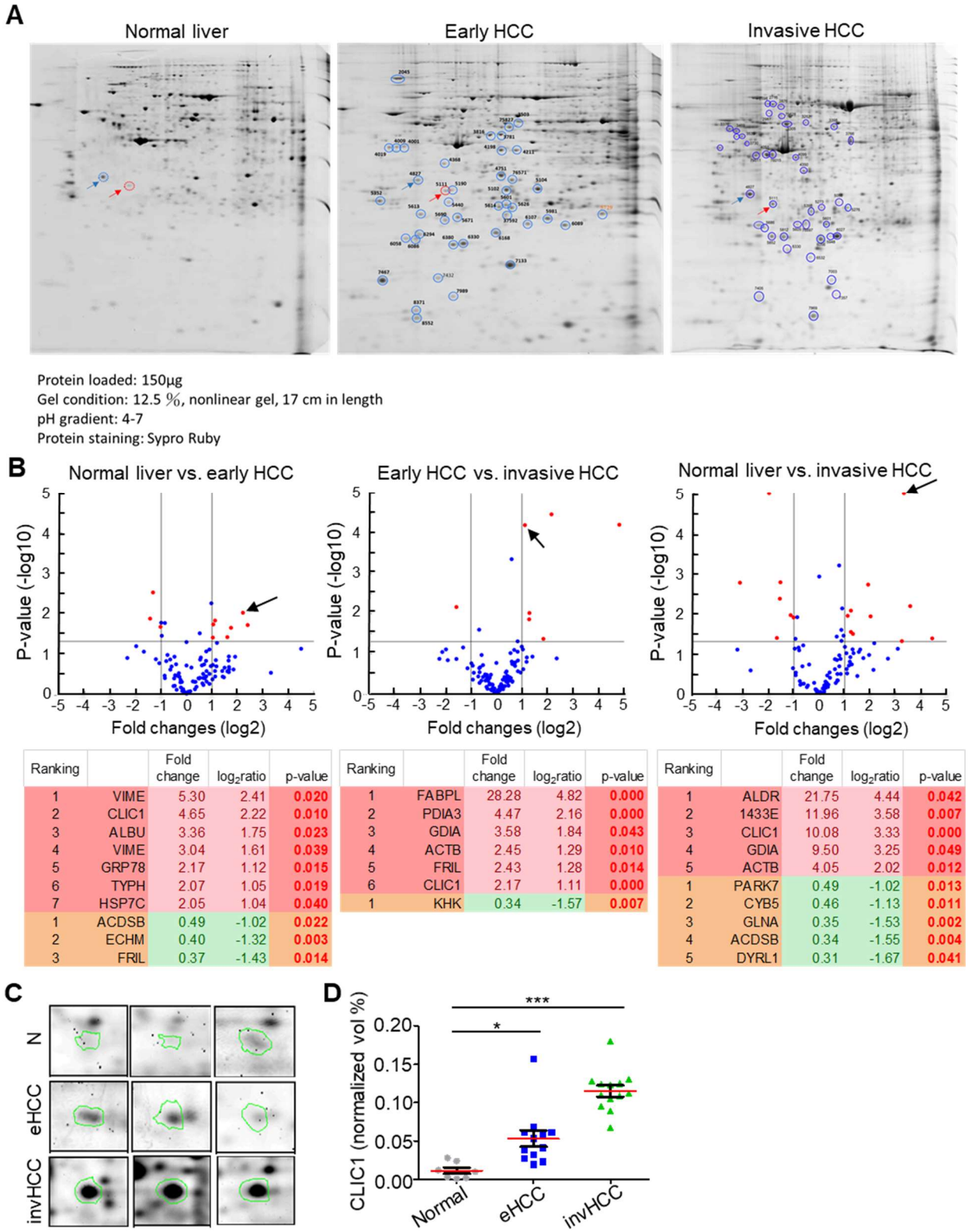

Ranking		Fold change	log_2ratio	p-value
1	VIME	5.30	2.41	0.020
2	CLIC1	4.65	2.22	0.010
3	ALBU	3.36	1.75	0.023
4	VIME	3.04	1.61	0.039
5	GRP78	2.17	1.12	0.015
6	TYPH	2.07	1.05	0.019
7	HSP7C	2.05	1.04	0.040
1	ACDSB	0.49	-1.02	0.022
2	ECHM	0.40	-1.32	0.003
3	FRIL	0.37	-1.43	0.014

Ranking		Fold change	log_2ratio	p-value
1	FABPL	28.28	4.82	0.000
2	PDIA3	4.47	2.16	0.000
3	GDIA	3.58	1.84	0.043
4	ACTB	2.45	1.29	0.010
5	FRIL	2.43	1.28	0.014
6	CLIC1	2.17	1.11	0.000
1	KHK	0.34	-1.57	0.007

Ranking		Fold change	log_2ratio	p-value
1	ALDR	21.75	4.44	0.042
2	1433E	11.96	3.58	0.007
3	CLIC1	10.08	3.33	0.000
4	GDIA	9.50	3.25	0.049
5	ACTB	4.05	2.02	0.012
1	PARK7	0.49	-1.02	0.013
2	CYB5	0.46	-1.13	0.011
3	GLNA	0.35	-1.53	0.002
4	ACDSB	0.34	-1.55	0.004
5	DYRL1	0.31	-1.67	0.041

Figure 1. Comparative proteomics identified CLIC1 progressively upregulated along with HCC progress. Liver samples, including seven normal livers (para-tumor liver from cases of hepatic focal nodular hyperplasia), 12 early HCCs, and 13 invasive HCC, were subjected to proteomics analysis. (**A**) Representative 2-D gel maps of normal liver, early HCC, and invasive HCC. Red arrows indicate

CLIC1 on 2-D gel maps. (**B**) Volcano plots present overviews of the proteins that differentially expression in healthy liver, early HCC, and invasive HCC. The log2 fold change and the negative $\log_{10}$ (FDR) are indicated on the x- and y-axis, respectively. Proteins with >2-fold changes and *p*-value < 0.05 were regarded as deregulated (red spots) and are summarized in lower panels. Arrows indicate CLIC1, which is the only protein that is progressively upregulated along with HCC progress. Statistical analysis was performed by Mann-Whitney *U* test. (**C**) Representative focal 2-D images show CLIC1 in normal liver, early HCC, and invasive HCC. (**D**) Dot plot of the normalized volumes of CLIC1 in normal liver, early HCC (eHCC), and invasive HCC (invHCC). Mean ± SD are shown. Statistical analysis was performed by one-way ANOVA with Dunnett's corrections. See also Supplemental Table 1 and 2.

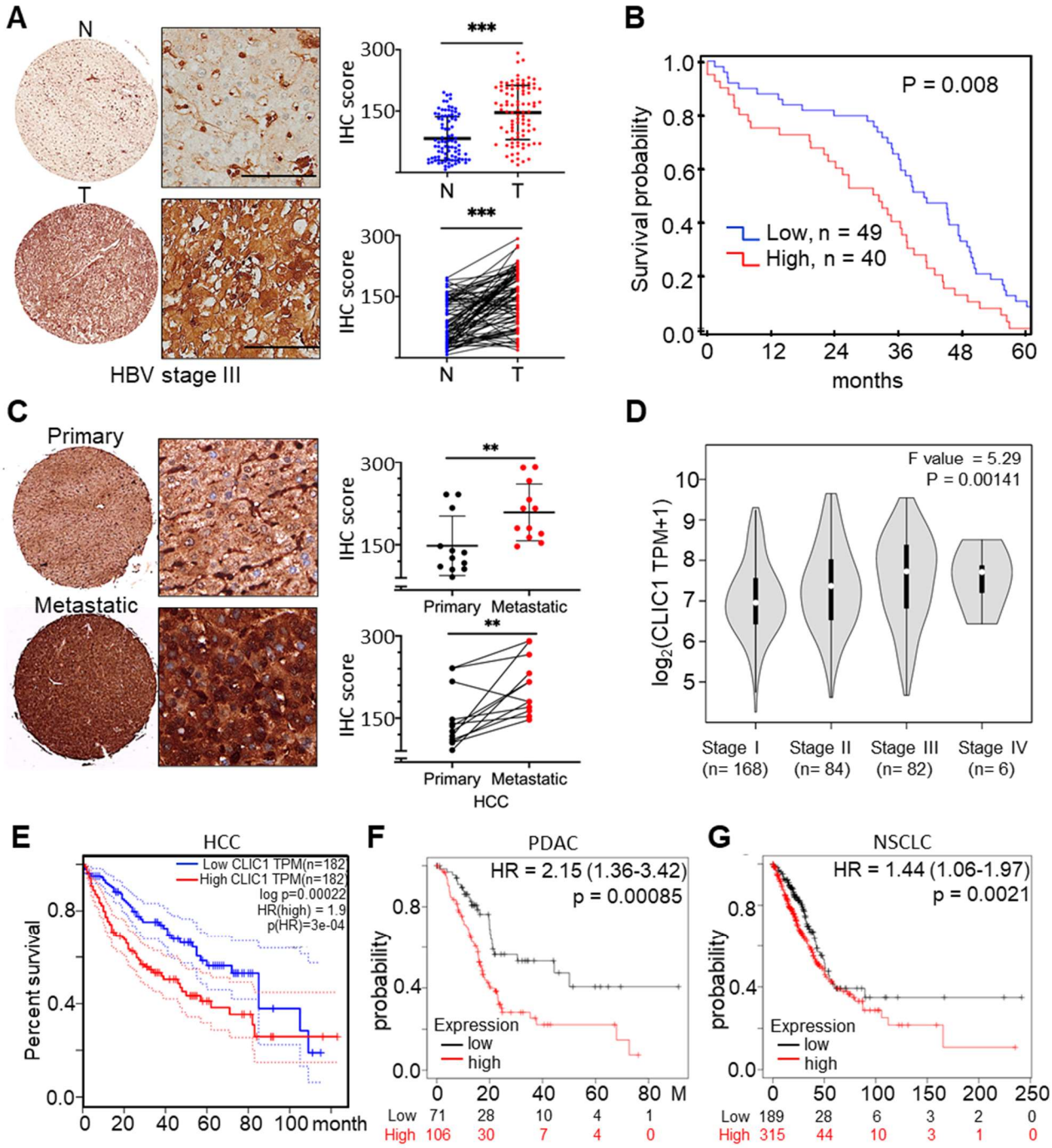

Figure 2. CLIC1 upregulation in HCC is associated with vascular invasion, metastasis, and lower survival. A total of 89 pairs of HCC (T) and para-tumor (N) liver tissues and 12 pairs of primary and metastatic HCCs were included. IHC scores for CLIC1 [= percentage of positive hepatocytes × IHC intensity (0-3)] were determined by an automation system (inForm® Advanced Image Analysis Software, version 2.3, PerkinElmer, MA). (**A**) A pair of representative IHC images of N and T. Scale bar = 100 μm. Dot plots show the comparison between N and T. Upper, two-tailed Student's *t*-test; lower, paired *t*-test. ***$P < 0.001$. (**B**) Kaplan-Meier survival curves for the 89 cases of HCC with high (IHC score ≥ 200, n = 40) and low (IHC score < 200, n = 49) CLIC1 levels. A log-rank test determined

p-value. (**C**) Representative IHC images of paired primary and metastatic tumors. Scale bar = 100 μm. Dot plots: Upper, Mann-Whitney *U* test; lower, Wilcoxon signed-rank test. ***P* < 0.01. (**D**) Violin plot shows the relative CLIC1 mRNA levels (central dots: medians; bold bars: interquartile ranges) in different stages of HCC in a TCGA HCC cohort (n = 370). Statistical analysis was performed by one-way ANOVA with Tukey's corrections. TPM: transcripts per kilobase million. (**E-G**) Kaplan-Meier survival curves generated from three TACG cohorts: HCC (n = 370), PDAC (n = 177), and NSCLC (n = 504). High and low CLIC1 levels were based on the median CLIC1 value for HCC and the optimal *P* values by log-rank tests for PDAC and NSCLC.

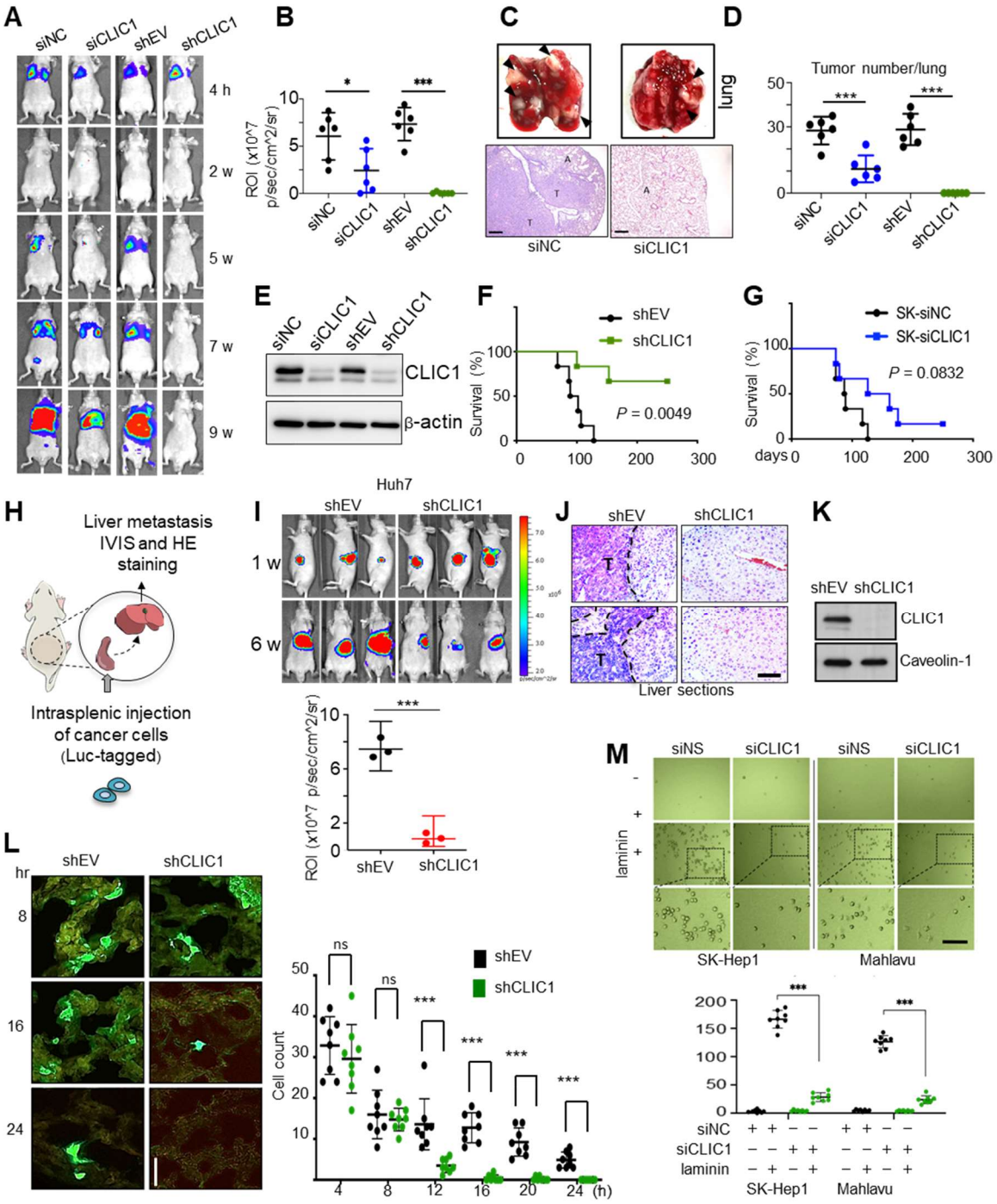

667

668 **Figure 3. CLIC1 facilitates adherence and extravasation of tumor cells for metastasis in mice.**
669 Luciferase-transduced SK-Hep1 and Huh7 cells were used for in vivo metastasis in nude mice. Cells
670 transfected with siRNAs containing scrambled sequences (siNC) or targeting CLIC1 (siCLIC1), or
671 constitutively transduced with shRNAs targeting CLIC1 (shCLCI1) or an empty vector (shEV). (**A**) Lung
672 metastasis assays by injecting SK-Hep1 cells (1 x 10^6 cells in 200 μL PBS/mouse, n = 6) through tail
673 veins. (**B**) The statistical results of the luminescence signals for lung metastasis. Statistical analysis
674 was performed by using Mann-Whitney *U* test between two groups (n = 6/group; **P* < 0.05; ****P* <

675 0.001). (**C**) Representative lung tissues 63 days after injection. Arrowheads, metastatic tumors.
676 Lower panel: Haematoxylin and eosin staining (H&E) for the lung sections. A: lung alveoli; T:
677 metastatic tumors. Scale bar = 120 μm. (**D**) Dot blot of metastatic tumor foci per lung. Statistical
678 analysis was performed by using Mann-Whitney *U* test between two groups (n = 6/group; ***P <
679 0.001). (**E**) Western blots for CLIC1 silencing efficiency in HCC cells. (**F** and **G**) Cumulative survival
680 curves for the mice bearing xenograft tumors. P values was determined by the log-rank test. (**H**)
681 Liver metastasis in nude mice by injection of luciferase-transduced Huh7 cells through the spleen. (**I**)
682 Liver metastasis was inspected by IVIS imaging at weeks 1 and 6 after injection. Lower panel:
683 Quantification of luciferase signals in the liver six weeks after injection. Statistical analysis was
684 performed by using Mann-Whitney *U* test (n = 6/group; ***P < 0.001). (**J**) H&E for liver sections.
685 Scale bar = 120 μm. (**K**) Western blots for CLIC1 silencing efficiency. (**L**) GFP-transduced SK-Hep1
686 cells with or without CLIC1 depletion were injected through tail veins. Lungs were assayed at 4, 8,
687 12, 16, 20, 24h after injection. Representative lung section images at 8, 16, and 24 h after injection
688 are shown. GFP-labeled tumor cells were detected and quantified. Statistical analysis was
689 performed by using Mann-Whitney *U* test between two groups (n = 8; NS: no statistical significance;
690 ***P < 0.001). (**M**) In vitro cell adhesion assays. The experiments were conducted twice
691 independently. Statistical analysis was performed by using two-tailed Student's *t* test between two
692 groups (n = 8/group; ***P < 0.001).
693

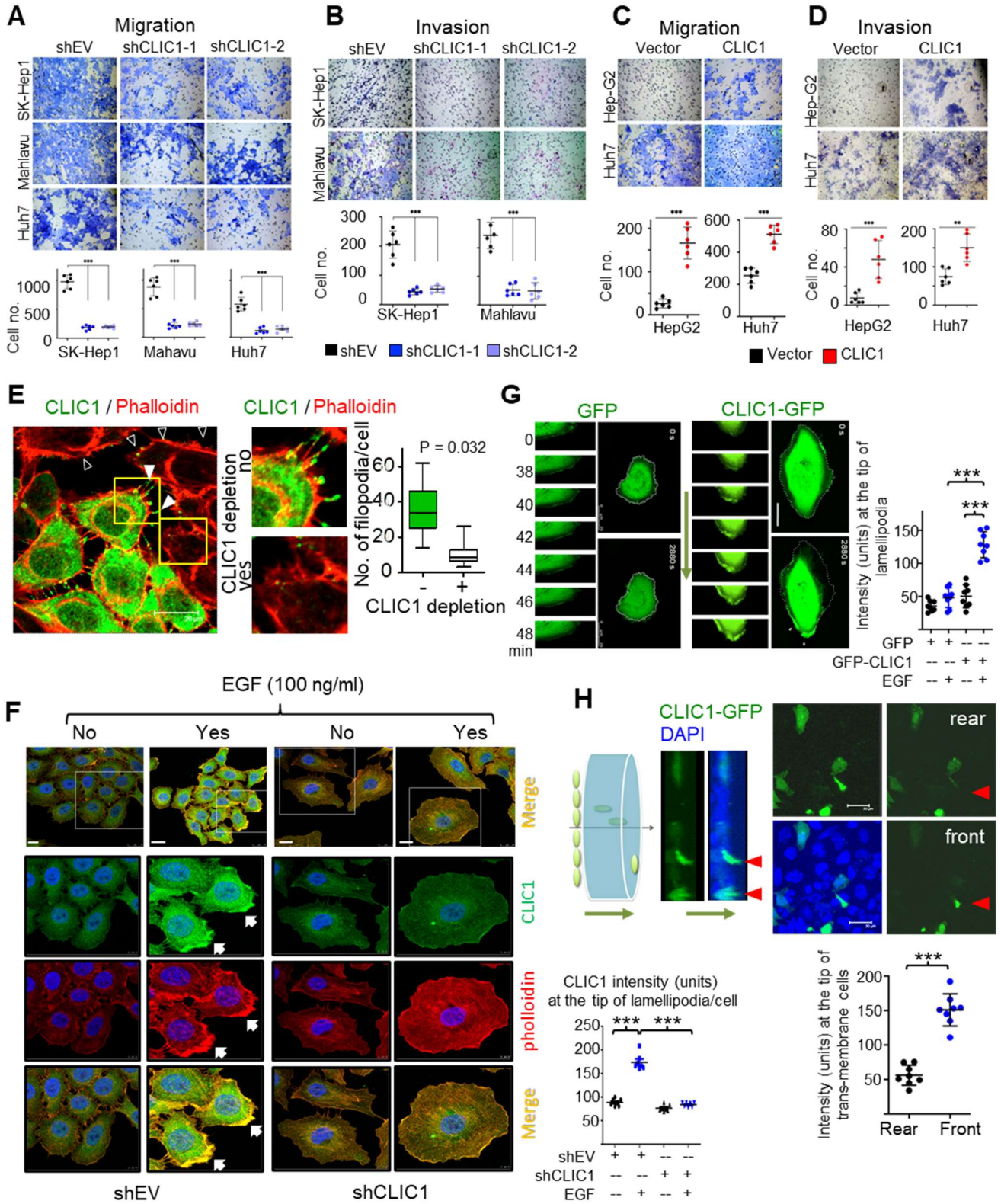

Figure 4. CLIC1 facilitates filopodia, lamellipodia, and invadopodia upon migration induction. (A-D) Transwell assays for migration and invasion (with Matrigel coating) of tumor cells with and without CLIC1 depletion (**A** and **B**), or with and without ectopic expression of CLIC1 (**C** and **D**). Two shRNA clones targeting CLIC1 mRNA were used. Vector: empty vector. Statistical analysis was

699 performed by using One-way ANOVA with Dunnett's test (A and B) or two-tailed Student's *t* test (n
700 = 6/group in triplicate; ***P* < 0.01; ****P* < 0.001). See also Supplemental Figure 3. (**E**) Huh7 cells
701 with (open arrowheads) vs. without CLIC1 depletion eight hours after free-space exposure. Green
702 (Alexa 488): endogenous CLIC1. Red (Alexa 549): F-actin. White arrowheads: CLIC1 accumulated at
703 the filopodia tips. Box plot: Relative numbers of filopodia per cell. P values were determined by
704 two-tailed Student's *t* test (n = 20 cells/group). (**F**) Huh7 cells with and without CLIC1 depletion
705 before and 10 min after EGF treatment. Arrows: CLIC1 at lamellipodia of migrating cells. Scale bars:
706 10 μm. Dot plot: the relative fluorescence intensity at the lamellipodia tips per cell. P values were
707 determined by using 2-way ANOVA with Tukey's corrections (n = 8 cells/group). (**G**) Time-lapse
708 tracking of GFP (upper panel) and CLIC1-GFP (lower panel) in Mahlavu cells in response to EGF
709 treatment. Images were taken every 2 min after EGF treatment. Arrow: migration direction. Scale
710 bar = 10 μm. Statistical analyses were performed by 2-way ANOVA with Tukey's corrections (n = 8
711 cells/group). (**H**) Three-dimensional invasion assays for CLIC1-GFP cells. Arrows: invasion direction.
712 Red arrowheads: the protruding edge of the invading cells. Arrow: migration direction. Dot plot
713 shows the fluorescence intensity (CLIC1-GFP) at the rear versus front tips of cells during passing the
714 matrix gel. Statistical analyses were performed by using two-tailed Student's *t* test (n = 8
715 cells/group).
716

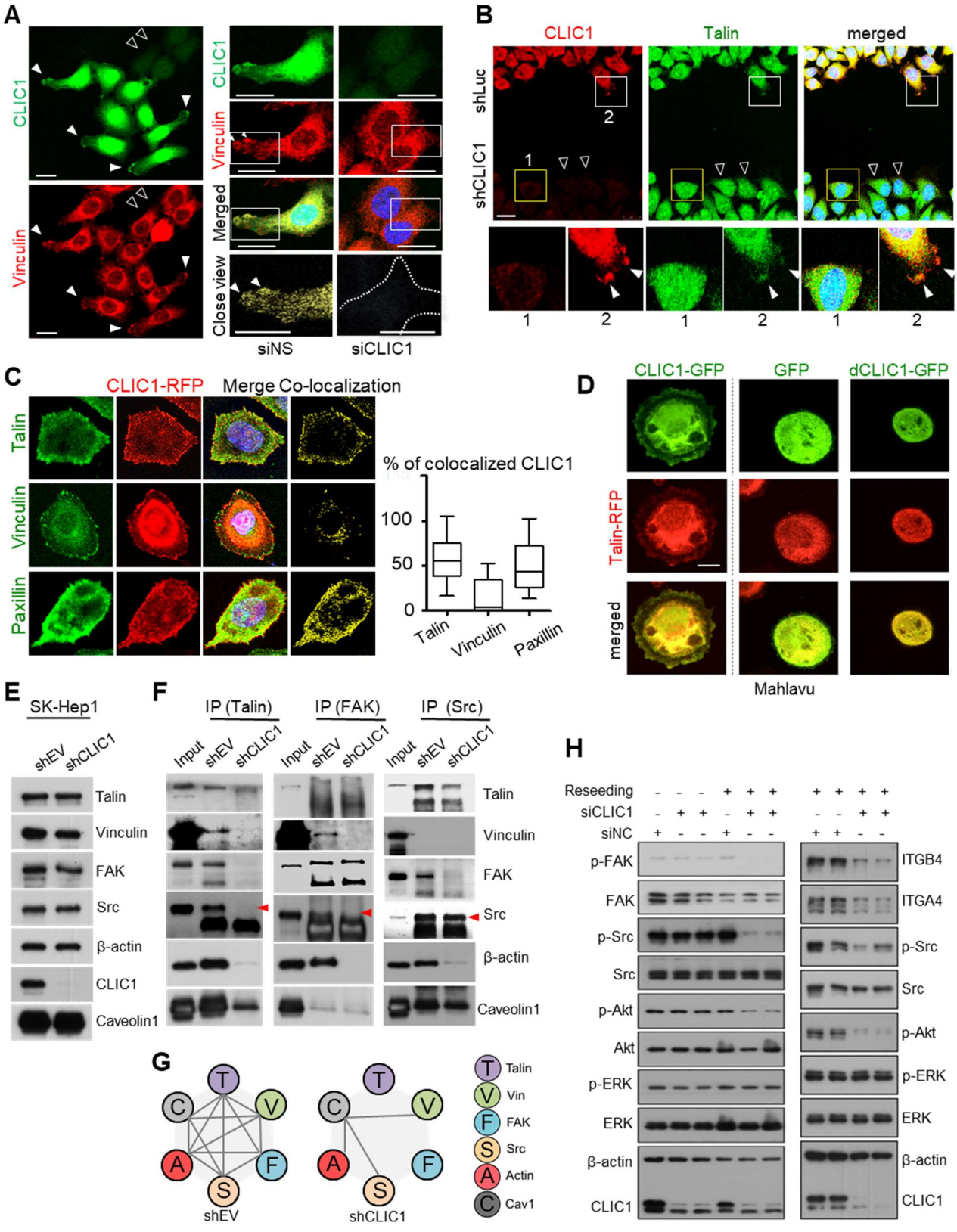

Figure 5. CLIC1 directs the formation of cell-matrix adhesions and signaling. (**A** and **B**) Nascent cell-matrix adhesions in lamellipodia of cells with and without CLIC1 depletion in response to (**A**) EGF treatment (10 min, 100 ng/ml) or (**B**) exposure to free space (8 h after wounding). White

721 arrowheads indicate the tips of lamellipodia. Open arrowheads indicate cells with CLIC1 depletion,
722 in which few lamellipodia and nascent adhesions were seen. Scale bar = 10 μm. (**C** and **D**) Confocal
723 images for the formation of nascent cell-matrix adhesions 15-30 min after cells reseeded on
724 laminin-coasted plates. See also Supplemental Figure 5A. (**C**) Red: CLIC1-RFP; green: talin-GFP,
725 vinculin-GFP, and paxillin-GFP. Box plots: the median and interquartile ranges of the amounts of
726 CLIC1 colocalized with talin, vinculin, and paxillin. (**D**) Colocalization of CLIC1-GFP but not dCLIC1
727 (deleted transmembrane domain) or GFP with talin at nascent cell-matrix adhesions. Scale bar = 5
728 μm. (**E**) Immunoblots show the effects of silencing CLIC1 on the talin, vinculin, FAK, Src, and actin
729 levels. (**F**) Coimmunoprecipitation assays using antibodies against talin, FAK, and Src to pull-down
730 binding proteins of SK-Hep1 cells with versus without CLIC1 depletion. Immunoblots with antibodies
731 to detect the key components of cell-matrix adhesions. See also Supplemental Figure 5B. Each assay
732 was performed independently at least twice. (**G**) Cartoons summarize the results from co-IP. (**H**)
733 CLIC1 selectively required for activation of nascent adhesion-mediated signals. Huh7 cells
734 transfected two different clones of siCLIC1 or a control siRNA (siNC). We compared the cells after
735 been reseeded (reseeding +) or in inactive status (reseeding -). Reseeding assays were used to
736 induce the formation of nascent cell-matrix adhesions.
737

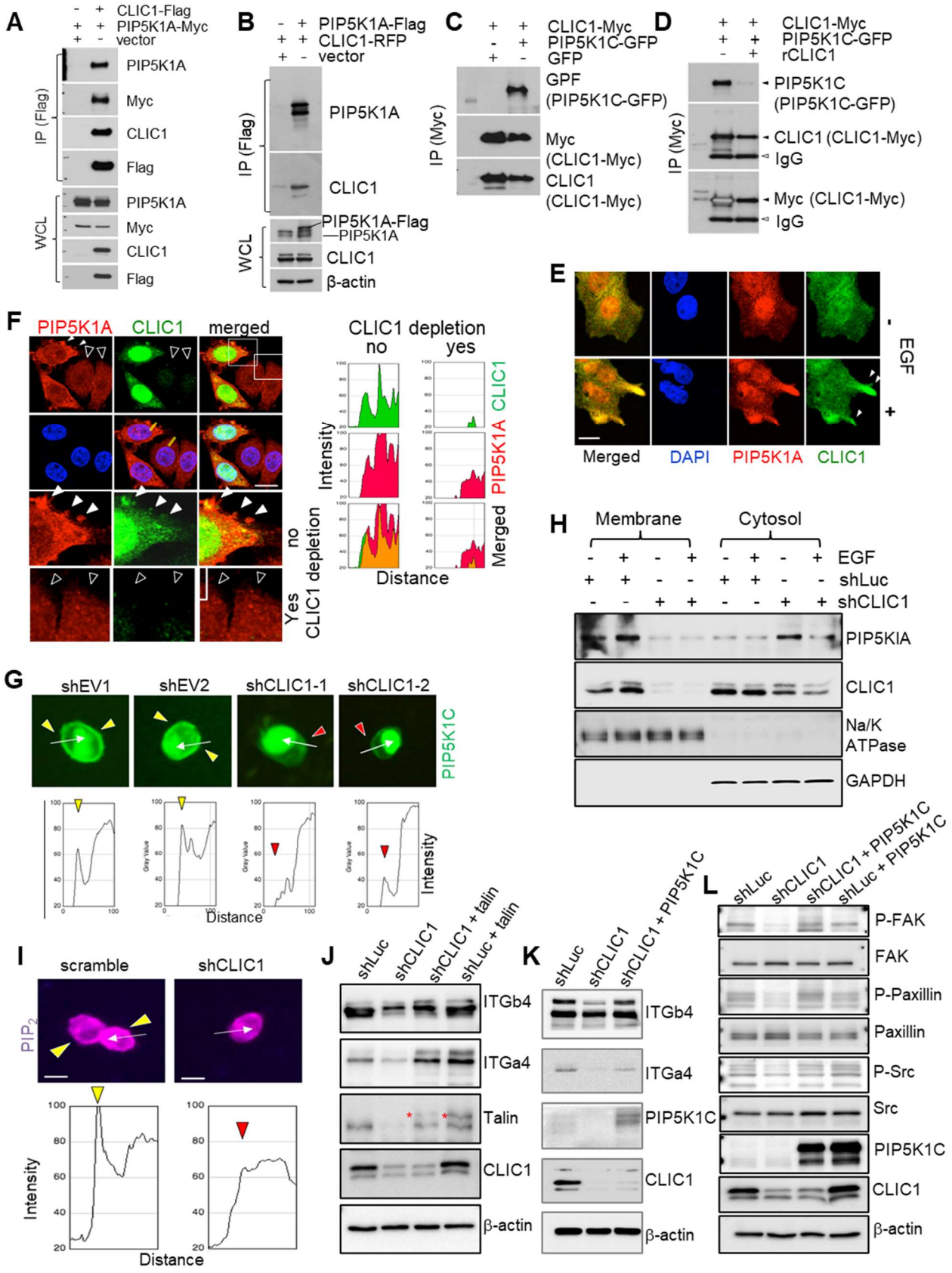

Figure 6. CLIC1 recruits PIP5K to the plasma membrane to initiate "PIP_2-talin-integrin"-mediated cell-matrix adhesion formation. (**A**-**D**) Immunoprecipitation (IP) by using antibodies against the

741 flag- or myc-tag. WCL: whole cell lysate as the loading control. (**A**) IP for CLIC1-bound proteins. (**B**) IP
742 for PIP5K1A-bound proteins. (**C**) IP for CLIC1-bound proteins. (**D**) The binding specificity was
743 examined by a recombinant CLIC1 (rCLIC1) before IP. (**E**) Immunofluorescence (IF) demonstrates co-
744 targeting of CLIC1 (Alexa 594, green) and PIP5K1A (Alexa 488, red) to the tips of lamellipodia in
745 Huh7 cells before and after EGF treatment (10 min, 100 ng/ml; indicated by arrowheads). (**F**) IF for
746 lamellipodia formation and colocalization of PIP5K1A with CLIC1 at the front edge of lamellipodia of
747 cells with versus without CLIC1 depletion after EGF treatment. Scale bars: 10 μm. (**G**) Confocal
748 images show CLIC1-dependent accumulation of PIP5K1C at the nascent cell-matrix adhesions of
749 cells after being reseeded. Lower panel: Fluorescence intensities recorded along the arbitrary lines
750 across the cell membrane. (**H**) Subcellular fractionation for membrane-associated versus cytosolic
751 proteins. Na/K ATPase was used as a membranous marker, GAPDH, a cytosolic marker. EGF
752 treatment: 100 ng/ml for 10 min. (**I**) GFP-PH-PLC, a PIP_2 biosensor, was used to measure the
753 intracellular concentration of PIP_2 (54). Scale bars = 10 μm. The fluorescence intensities were
754 recorded along the arbitrary lines across the plasma membrane. (**J**-**L**) Ectopic expression of talin (**J**)
755 or PIP5K1C (**K** and **L**) prevented the suppression of integrin-α4 and β4 (**J** and **K**) and the nascent
756 adhesion-mediated signals (**L**) in CLIC1-depletion cells 45 min after reseeding.
757

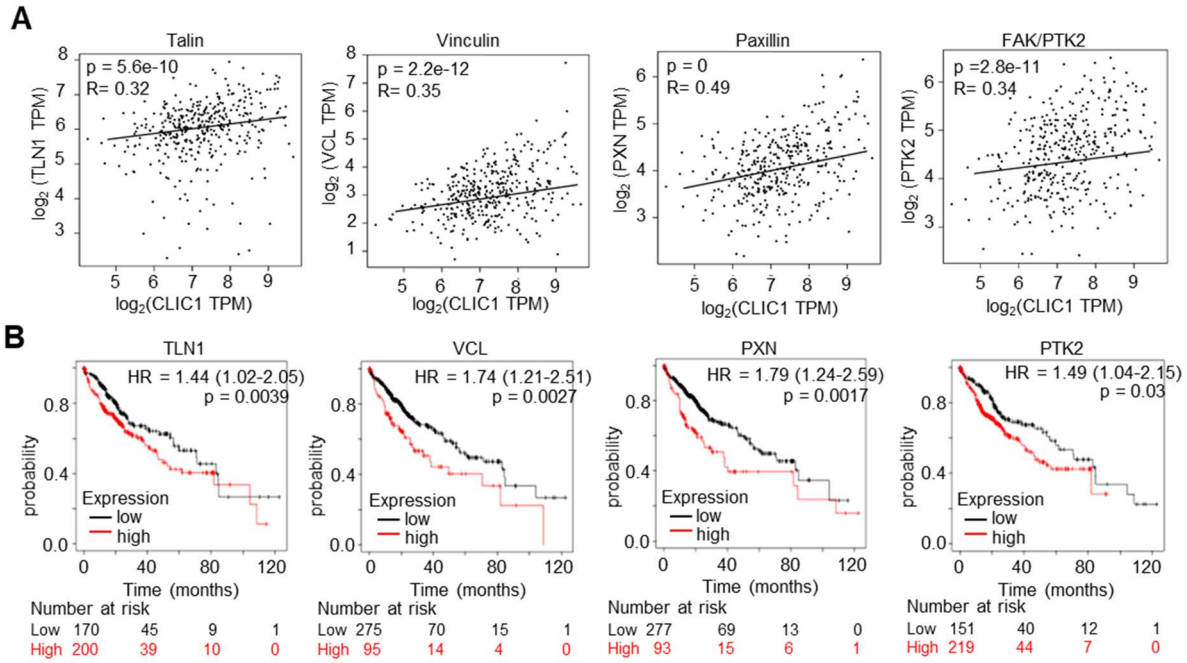

Figure 7. The expression levels of adhesion-related effectors predict poor clinical outcomes in HCC. A cohort of 370 cases of HCC was retrieved from TCGA. (**A**) The mRNA levels of cell-matrix adhesion markers, including talin, vinculin, paxillin, and FAK, were correlated to the CLIC1 mRNA levels by using the Pearson correlation. (**B**) Kaplan-Meier curves and log-rank tests for the probability of survival of 370 patients of HCC with high and low expression levels of talin (TLN1), vinculin (VCL), paxillin (PXN, and FAK (PTK2) in HCC patients. Stratification of patients into low- and high-expression subgroups was based on the optimal P values, which were determined by the log-rank tests.

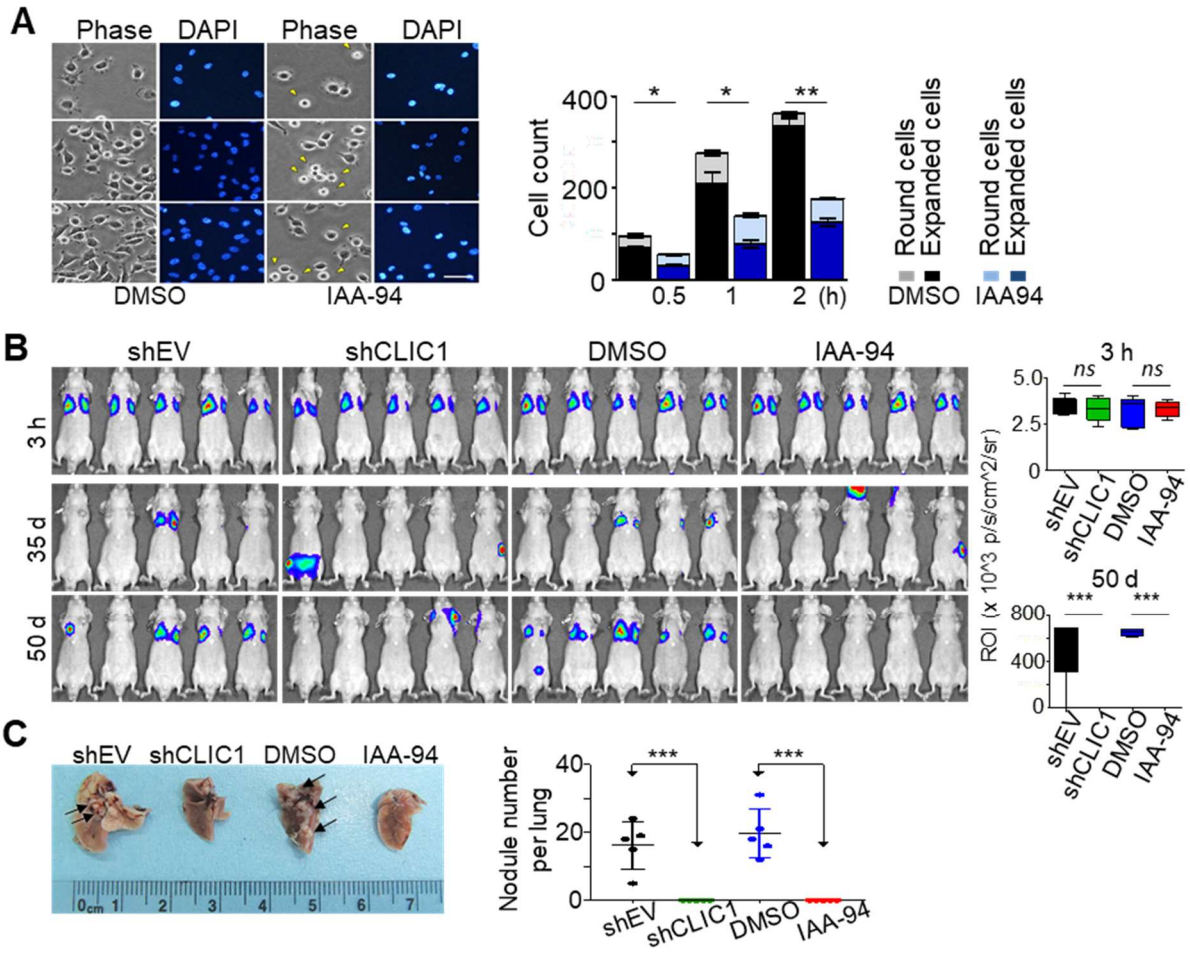
A
Phase
DAPI
Phase
DAPI
DMSO
IAA-94
Cell count
400
200
0
*
*
**
0.5
1
2 (h)
Round cells
Expanded cells
DMSO
Round cells
Expanded cells
IAA94
B
shEV
shCLIC1
DMSO
IAA-94
3 h
35 d
50 d
3 h
ns
ns
5.0
2.5
0
shEV
shCLIC1
DMSO
IAA-94
50 d
***
***
800
400
0
ROI (x 10^3 p/s/cm^2/sr)
C
shEV
shCLIC1
DMSO
IAA-94
Nodule number per lung
40
20
0
***
***
shEV
shCLIC1
DMSO
IAA-94
D
Chemokines
CLIC1
PIP2
1
PIP5K
α
β
2
Talin
Paxillin
Vin
3
FAK
SRC
F-actin
CLIC1
α
β
Talin
Vin
G-actin
Inactive status
In response to stimuli
Aberrant CLIC1 upregulation in tumors
CLIC1
PIP5K
Plasma membrane
PIP2
tailn
ITGs
Nascent adhesions
Adhesion
FAK/Src signaling
F-actin
Membrane protrusion
Directional migration

Figure 8. CLIC1 and its ion conductance are therapeutic targets for tumor metastasis. (**A**) IAA-94 reduced cell adherence. Yellow arrowheads: partially spread cells, representing a failure in adherence to the stratum. Scale bar = 50 μm. Statistical analysis was performed by using two-tailed Student's *t* test between two groups (four fields/dish, two independent experiments. *P < 0.05; **P < 0.01). (**B**) Xenograft lung metastasis monitored by Xenogen IVIS at different time points after injection of luciferase-transduced SK-Hep1 cells via the tail veins. Right panels: The box and whisker plots show the mean and interquartile ranges of the tumor-associated fluorescence intensity 3 h (upper) or 50 days (lower) after the injection. Statistical analysis was performed by using Mann-Whitney *U* test between two groups (n = 5 mice/group; ns = no statistical significance; *** P < 0.001. (**C)** Left panel: representative lung-tissues. Arrows indicate tumor nodules. Right panel: the dot plot. Statistical analysis was performed by using Mann-Whitney *U* test between two groups (n = 5 mice/group). (**D**) Schematic of the CLIC1-directed "PIP5K-PIP2-talin-integrin" signaling pathway to initiate the assembly and signaling of nascent cell-matrix adhesions. Left: at inactive status; right: in response to chemo- or mechanotaxis, or in tumors with aberrant upregulation of CLIC1. Aberrant upregulation of CLIC1 leads to the "PIP5K-PIP_2-talin-integrin" signaling to promote tumor invasion and metastasis.